Combination of Adsorption-Diffusion Model with Computational Fluid Dynamics for Simulation of a Tubular Membrane Made from SAPO-34 Thin Layer Supported by Stainless Steel for Separation of CO_2 from CH_4

Fatemeh Sadat Banitaba, Zahra Mansourpour and Shohreh Fatemi[*]

School of Chemical Engineering, College of Engineering, University of Tehran, Iran

Abstract: Modeling of CO_2/CH_4 separation using SAPO-34 tubular membrane was performed by computational fluid dynamics. The Maxwell-Stefan equations and Langmuir isotherms were used to describe the permeate flux through the membrane and the adsorption-diffusion, respectively. Three-dimensional Navier-Stokes momentum balances in feed and permeate side coupled with adsorption-diffusion equations from the membrane were simultaneously solved by ANSYS FLUENT software. The velocity and concentration profiles were determined in both feed and permeate sides. There was a good agreement between simulation and experimental results and root mean square deviation for CH_4 and CO_2 are 0.13 and 0.1 (mmol m^{-2} s^{-1}), respectively. The concentration polarization effect was observed in the results. The effect of the process variables were investigated to find out the most influential parameters in permeation and purity. The impact of operating conditions on separation were studied and showed that for enhancement of separation efficiency of CO_2 from CH_4, feed pressure, feed flow rate and tube radius and number of membrane modules in series should be increased, whereas flow configuration has less significant effect.

Keywords: Computational fluid dynamic, tubular zeolite membrane, CO_2/CH_4 separation, SAPO-34, Adsorption-diffusion mechanism.

INTRODUCTION

Methane as the major component of natural gas usually contains carbon dioxide impurity with a broad range of 2% up to 40 % in different sources, which must be removed because it reduces the energy content of the gas and because of its acidic and corrosive effects. The pipeline specifications for natural gas require a CO_2 concentration below 2–3% [1]. For separation of CO_2 from natural gas, several technologies, such as absorption, adsorption, cryogenic and membrane separation, have been investigated and used in recent years [2]. The advantages of membrane gas separation over traditional techniques include low-energy consumption, ease of operation, and low environmental impacts [3]. Polymeric membranes are commercially available for CO_2 separation from natural gas, but the main problem that limits the use of these membranes, is their poor performance stability at high pressure and in the presence of highly soluble components. Because of good thermal, mechanical, and chemical stability, zeolite membranes potentially have advantages over polymeric membranes. SAPO-34 is one of the micropore zeolite like material with Chabazite natural zeolite structure that displays high CO_2/CH_4 selectivity

due to a combination of differences in diffusivity and competitive adsorption [4]. SAPO-34 crystals with 0.38 nm micropore diameter act as a molecular sieve for CO_2 with 0.33 nm kinetic diameter. CO_2 can adsorb and diffuse through the crystalline surface of SAPO-34 whereas methane with 0.38 nm diameter is hindered by the pore mouth of SAPO-34 to diffuse and adsorb through the crystalline micropores [5].

Computational techniques have the potential of improving the understanding of mass transfer in membrane separation systems. Computational fluid dynamics (CFD) is one of the numerical techniques used for simulating fluid flow and is a powerful tool in engineering systems. It could enable to understand the fluid flow in membrane separation processes, and help to optimize the design conditions.

CFD has been generally applied in membrane processes involving the separation of liquids [6, 7]. Although researches on CFD modeling for gas separation membrane are limited, in the recent years with development of membrane material for gas separation, application of the CFD technique for gas separation modeling has been increased [8-16]. Koukou *et al.* [8] and Takaba and Nakao [9] reported that the simplified plug flow assumption on both sides of the ceramic membrane does not allow properly predicting the experimental data and does not show concentration polarization effects. Abdel-jawad *et al.* [10] used the phenomenological equations to describe

*Address correspondence to this author at the School of Chemical Engineering, College of Engineering, University of Tehran, Iran; Tel: + 98 21 66967784; Fax: + 98 21 66967784; E-mail: shfatemi@ut.ac.ir

the mass flux through the membrane. Kawachale *et al.* [11] have focused on the species distribution close to a polymeric membrane for VOC separations and described mass transfer through membrane by simple Fick equation. Coroneo *et al.* [12, 13] presented a three dimensional geometry to model H_2 purification in the ceramic and metallic membranes modules using CFD. Recently, Ji *et al.* [14, 15] simulated a multi tube COxS membrane with CFD approach in one- [14] and two-dimension(s) [15]. They used Maxwell-Stefan equation formulation to describe membrane mass transfer. Li *et al.* [16] simulated an axisymmetric BSCF ($Ba_{0.5}Sr_{0.5}Co_{0.8}Fe_{0.2O3-\delta}$) membrane for O_2/N_2 separation with a two dimensional fluent simulation and investigated the concentration polarization of oxygen. They concluded that with increasing sweep flow rates, the effect of concentration polarization is less pronounced.

In this study, the CFD approach is coupled with the Maxwell-Stefan equations to reveal the local variation of carbon dioxide and methane concentration and gas velocity profile near the membrane surface as a result of CO_2 and CH_4 permeations. The predicted model results of CO_2 and CH_4 permeations are compared with the experimental results obtained from a tubular SAPO-34 membrane in a lab scale. Moreover, effects of variations in operating variables include feed pressure, feed flow rate, flow configuration, membrane tube radius, and number of membranes in series are investigated.

EXPERIMENTAL DATA

The zeolite membrane was prepared as reported by Jabbari *et al.* [17]. Porous tubular stainless steel was used as a support with 9 and 10 mm internal and external diameter, respectively. The SAPO-34 film was grown on the inner surface of the support with the mean layer thickness of 4 µm. Membrane module consists of a cylindrical shell with a length of 70 mm and a diameter of 16.4 mm, equipped with inlet and outlet pipes having a diameter of 3.2 mm, and of an internal tube, containing the tubular zeolite membrane. A scheme of membrane module is shown in Figure **1**. Feed enters the tube and permeate flow exits from the shell side. No sweep gas was used in the permeation tests, thus the inlet valve of the sweep gas was blocked during experiments. The permeate side was kept at atmospheric pressure, feed side pressure varied from 1-6 barg and experiments were carried out at room temperature of 25°C. Equimolar mixture of CO_2/CH_4 was fed to the membrane module. The schematic

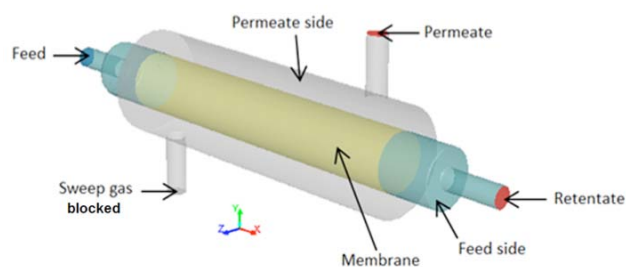diagram of the permeation test setup has been shown in Figure **2**.

Figure 1: A scheme of membrane module.

1-Pressuer regulator
2-Mass flow controller (MFC)
3-Mixing part
4-Niddle valve
5-Membrane module
6-Gas chromatograph
7-Gas flow meter
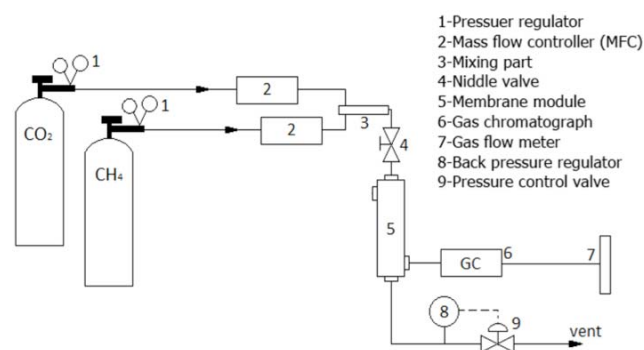8-Back pressure regulator
9-Pressure control valve

Figure 2: A schematic diagram of the permeation test setup.

MODEL DEVELOPMENT

CFD Model

In order to simulate the laminar flow of the gas mixture in the feed and permeate side of membrane module, the steady-state mass and momentum conservation equations over the three-dimensional domain were derived and solved. Also, a set of gas species conservation equations were solved to account for the separation. In addition, source terms were used to describe species transfer through the membrane film. The governing equations, based on the physical principles of continuity, momentum conservation and solutes conservation are shown in equations 1 to 3.

Mass conservation equation (continuity):

$$\nabla.(\rho U) = S \tag{1}$$

Momentum conservation equation (Navier-stokes):

$$\nabla.(\rho UU) = -\nabla P + \nabla.\tau \tag{2}$$

Species conservation equation:

$$\nabla.(\rho UY_i) = -\nabla.(\rho D\nabla Y_i) + S_i \tag{3}$$

Where ρ is the density, U is the velocity vector, τ is the viscous stress tensor, P is the pressure, S and S_i are source terms to account for the total mass flow and mass flow of species i through membrane, respectively. It must be noted that all source terms in equations 1 to 3 are zero everywhere in solution domain, except at the interface with the membrane where the source matches with the total membrane flux.

Source Term Formulation

In this section, the theory of Maxwell-Stefan is developed for demonstration of diffusion through the zeolite membrane, which would be applied for prediction the source term in the model equations.

The species flux and total flux through the membrane were considered as follows:

$$S_i = M_i \frac{A_c}{V_c} J_i \tag{4}$$

$$S = \sum S_i \tag{5}$$

Where A_c is the cell area, V_c is the cell volume and M_i is molecular mass i species. A mathematical model was developed to describe the mass transfer through zeolite film on the basis of the following assumptions: (i) the effect of support layer and defects of the zeolite film are neglected (ii) the transport of the absorbing components through the zeolite membrane occurs due to adsorption-diffusion, described by the Maxwell-Stefan model and (iii) gas translational diffusion is neglected due to the low temperature. Permeation flux of single component trough zeolite film with the single-site Langmuir adsorption isotherm is [18]:

$$J = q_{sat} \frac{\rho_z D}{\delta} \ln \frac{1 - \theta_{perm}}{1 - \theta_{feed}} \tag{6}$$

$$\theta = \frac{q}{q_{sat}} = \frac{bP}{1 + bP} \tag{7}$$

Where D is Maxwell–Stefan diffusivity and θ is coverage fraction. the permeation flux through membrane for a mixture could be described with generalized Maxwell-Stefan formulation [19] as follows:

$$J = \rho_z [q_{sat}][B]^{-1}[\Gamma](\nabla\theta) \tag{8}$$

Where $[B]$ is Maxwell–Stefan diffusivity matrix and $[\Gamma]$ is thermodynamic matrix. The values of these matrixes are obtained from:

$$B_{ii} = \frac{1}{D_i} + \sum_{\substack{j=1 \\ j \neq i}}^{n} \frac{\theta_j}{D_{ij}}, B_{ij} = \frac{-\theta_i}{D_{ij}}, \Gamma_{ij} = \frac{\theta_i}{P_i} \frac{\partial P_i}{P i \partial \theta_j} \tag{9}$$

To relate coverage fraction, θ_i to the partial pressure, two models could be used, including ideal adsorption solution theory (IAST) [20] and multicomponent Langmuir isotherm [21]. In this work, we used multicomponent Langmuir model for binary mixture, thus we have:

$$\theta_i = \frac{q_i}{q_{i,sat}} = \frac{b_i P_i}{1 + \sum_{j=1}^{2} b_j P_j} \tag{10}$$

For ease of numerical calculation, linear profile for coverage fractions were considered, thus the fluxes can be written as:

$$J_1 = q_{sat,1} \frac{\rho_z D_1}{\delta} \frac{(1 - \theta_2 + D_2/D_{12}\theta_1)\Delta\theta_1 + (\theta_1 + D_2/D_{12}\theta_1)\Delta\theta_2}{(1 + D_2/D_{12}\theta_1 + D_1/D_{12}\theta_2)(1 - \theta_1 - \theta_2)} \tag{11}$$

$$J_2 = q_{sat,2} \frac{\rho_z D_2}{\delta} \frac{(1 - \theta_1 + D_1/D_{12}\theta_2)\Delta\theta_2 + (\theta_2 + D_1/D_{12}\theta_2)\Delta\theta_1}{(1 + D_2/D_{12}\theta_1 + D_1/D_{12}\theta_2)(1 - \theta_1 - \theta_2)} \tag{12}$$

CFD SIMULATION DETAILS

Model development and simulations were performed using ANSYS FLUENT® 13.0 commercial CFD software and GAMBIT 2.2. The geometrical configuration of the simulated apparatus was as described in experimental data section. The computational domain consists of about 506000 hexahedral and tetrahedral elements. The membrane in the domain was defined as shadowed wall, while all other edges represent the barriers of the remaining cell geometry. Boundary conditions for feed, sweep gas permeate and retentate streams were obtained from empirical data as velocity inlet and pressure outlets, respectively and are listed in Table **1**. Viscous model was set to 'Laminar', and the discretization of the governing equations was performed using a segregated incompressible flow solver. The Semi-Implicit Method for Pressure-Linked Equations

Table 1:   Defined Boundary Condition for Geometry

Stream name	Boundary condition	value
feed	velocity inlet mole fraction	0.125 m/s 0.5
sweep gas	velocity inlet	0 m/s
permeate	pressure outlet	0 bar gauge
retentate	pressure outlet	1-6 bar gauge

(SIMPLE) formulation of pressure-velocity coupling was used to obtain the required corrections to the pressure and velocity fields. The convergence criteria for the continuity and velocity parameters were fixed to 10^{-5}. Pressure was set to 'Linear' and momentum was set to 'Second Order Upwind' discretization schemes for more accurate results [22].

User Defined Function (UDF)

As mentioned above, equations 1 to 3 were solved to specify fluid dynamics and source terms in those equations describing transport of gas through the membrane. The source terms were achieved using a series of user defined functions (UDFs) in ANSYS FLUENT® software according to the formulation in the CFD model section. Figure **3** shows the flowchart of the numerical solution procedure. After initializations and boundary conditions setting, source terms were calculated from cells near to membrane walls in both feed and permeate sides by a DEFINE_ADJUST macro. These sources were added to continuity and species conservation equations by two DEFINE_SOURCE macros.
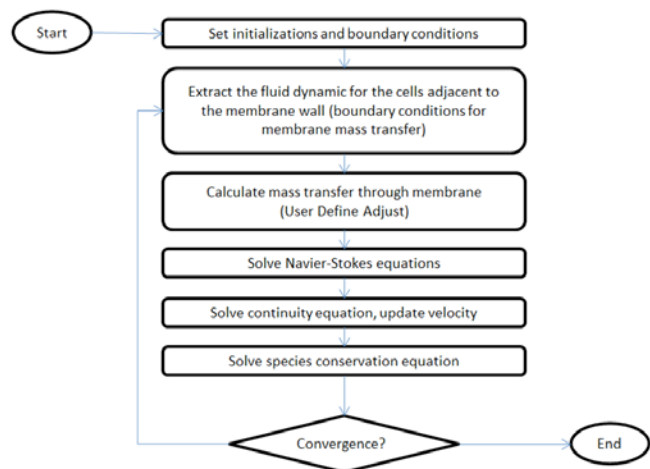

Figure 3: The flowchart of the numerical solution procedure.

RESULTS AND DISCUSSION

Model Validation

Figure **4** shows the experimental CH_4 and CO_2 fluxes from the permeate side, as a function of pressure drop across the membrane. The points are the experimental data. For both gases the fluxes continuously are increased with pressure difference. Other researchers have reported similar behaviors for these gases through SAPO-34 membranes when pressure drop is increased [23]. Figure **4** also shows the result obtained from simulation with continues lines.

As can be seen they have good agreement with experimental data. Root mean square deviation for CH_4 and CO_2 are 0.13 and 0.1 (mmol m^{-2} s^{-1}), respectively. CO_2 mole fraction at permeate for these cases are shown in Figure **5** and in which experimental and model results could be compared.
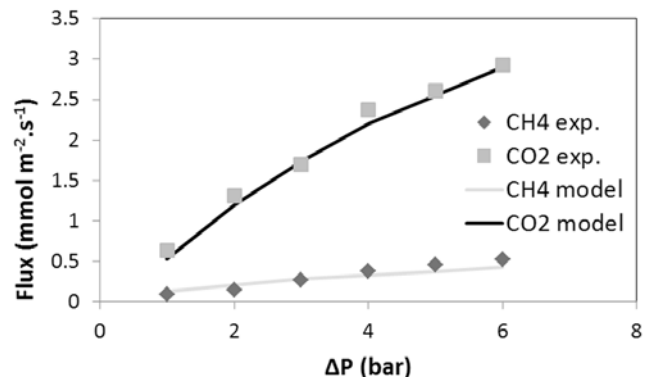

Figure 4: CH_4 and CO_2 fluxes from the permeate side, as a function of pressure drop across the membrane.
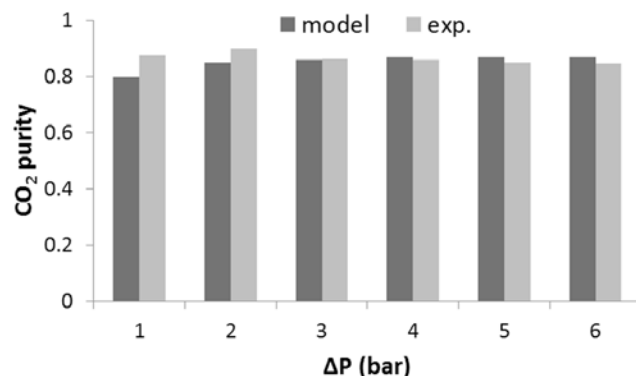

Figure 5: CO_2 mole fraction at permeate as a function of pressure drop.

In addition, simulation results could be shown in graphical view with velocity and concentration maps on the arbitrary sections of geometry such as z=0 (see Figure **6a**). Figure **6b** shows velocity vector in this plane. Direction of vectors near the membrane wall clearly shows the direction of mass transfer through membrane. In addition, Figure **6b** shows gas stream which enter from the feed inlet, exit from the retentate outlet and a portion of it diffuses through membrane and exit from the permeate outlet.

Figure **7a** illustrates the CO_2 mole fraction profile at feed side on the z=0 plane. It can be seen from the mole fraction map that CO_2 mole fraction has shown dispersion in both radial and axial directions. It is clear that CO_2 molecules permeate from the membrane more than CH_4 molecules do, therefore mole fraction of
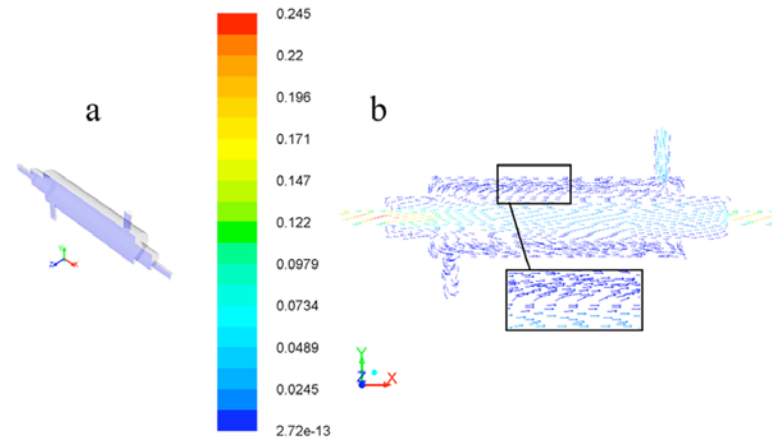
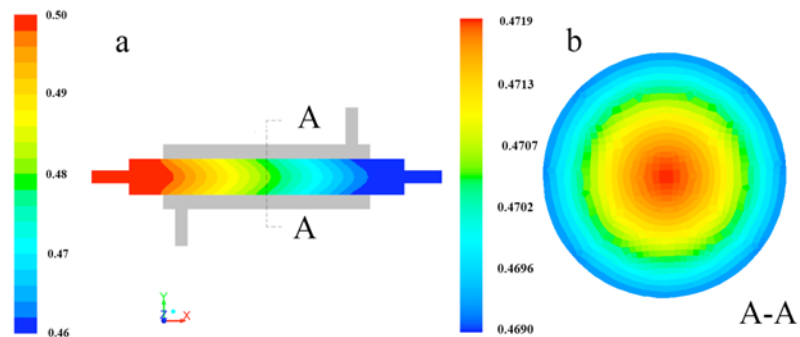**Figure 6: a**) Velocity map on the sections of geometry z=0, **b**) velocity vector in this plane.

Figure 7: a) The CO_2 mole fraction profile at feed side on the z=0 plane, **b**) Radial profile of CO_2 mole fraction.

CO_2 is decreasing in the axial direction. Radial profile of CO_2 mole fraction is also showed in Figure **7b**. As can be seen, CO_2 mole fraction near the membrane wall is decreasing due to permeation through membrane and it shows concentration polarization effect at the feed side. However, the low flux through the membrane weakens this effect.

Figure **8** shows CO_2 mole fraction profile at the permeate side. CO_2 mole fraction decreases along the
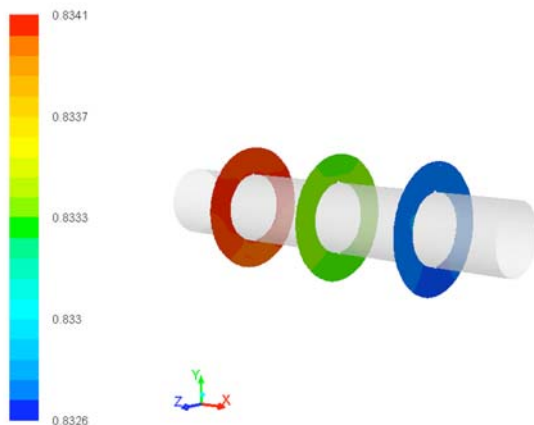

Figure 8: CO_2 mole fraction profile at the permeate side.

axis at permeate side. As CO_2 molecules permeate from feed side to the permeate side, CO_2 content is reduced in feed side, thus by decreasing driving force, CO_2 content would be reduced in permeate side.

Sensitivity Analysis

For understanding the impact of variation of operational variables and module design parameters on CO_2 permeation flow rate and mole fraction, some additional simulation should be performed. The changes in operating conditions were investigated as follows.

Feed Pressure

To estimate the effect of feed pressure on separation process, simulations were performed with two pressures of 4 and 8 barg in feed side while feed flow rate remain constant. Results are shown in Figure **9**. In Figure **9a**, as it was expected, pressure has significant impact on CO_2 permeate flow rate and increased with pressure difference because the pressure difference is considered as a driving force for permeation through the membrane. Figure **9b** shows a small effect on the CO_2 mole fraction at the permeate
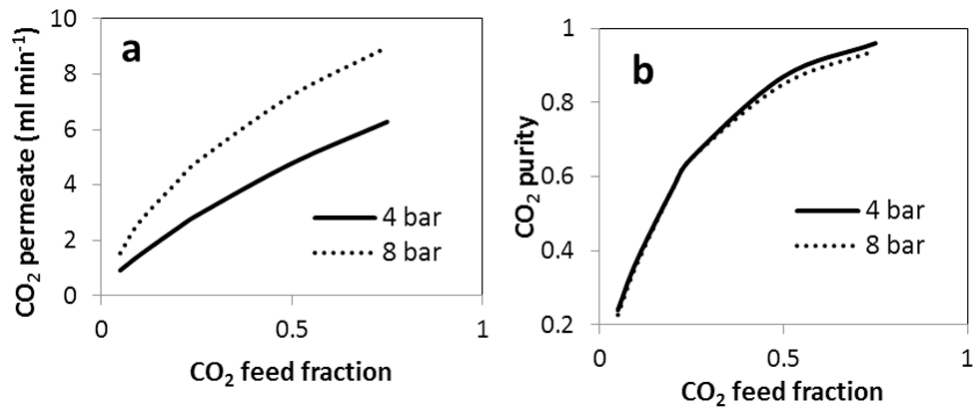
Figure 9: a) CO_2 permeate flow rate at various pressure difference, **b**) CO_2 mole fraction at the permeate Side at various pressure difference.
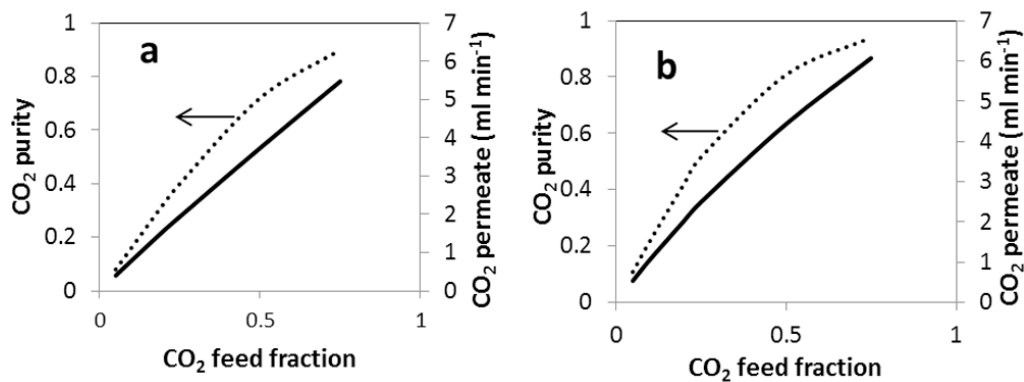

Figure 10: The effect of feed flow rate on separation process at different feed flow rates **a**) 10 mL/min and **b**) 20 mL/min.

side. It is clear that driving forces increase for both CO_2 and CH_4 permeation by increasing feed pressure, therefore CO_2 fraction remains approximately constant between 4 to 8 barg.

Feed Flow Rate

The effect of feed flow rate on separation process was investigated with simulation of two feed flow rates of 10 and 20 mL/min and results are shown in Figure **10a** and **b**, respectively. With comparison of two figures it could be seen that CO_2 permeation flow rate increase with feed permeation flow rate due to CO_2 inlet increase, furthermore CO_2 purity has small change with increasing feed flow rate, which is expected because driving force for both CO_2 and CH_4 would be increased.

Flow Configuration

Two different flow configurations were considered: In the first configuration permeate outlet was near the feed and in other case it was considered near retentate outlet. Permeate mole fraction and flow rate in two different flow configurations and two different feed fractions are listed in Table **2**. Comparison of two configurations showed that flow configuration has a small effect on permeation flow and fraction, and the results exhibit better separation efficiency in the first configuration.

Membrane Tube Radius

The effect of membrane tube radius on permeate fraction and flow rate is shown in Figure **11**. Figure **11a**

Table 2:   Effect of Flow Configuration on Permeate Mole Fraction and Flow Rate; with Feed Pressure of 4 Barg

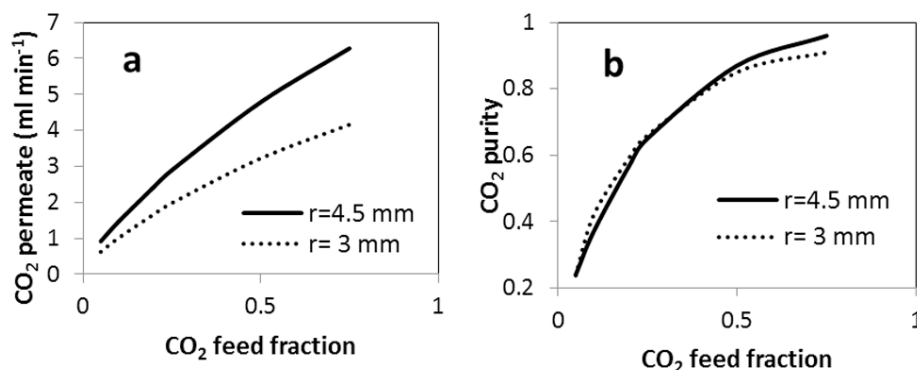|	CO_2 feed fraction: 0.25		CO_2 feed fraction: 0.75	
	configuration I	configuration II	configuration I	configuration II
CO_2 purity	0.65	0.58	0.96	0.95
CO_2 permeate (mL min^{-1})	2.89	2.85	6.28	6.26

Figure 11: The effect of membrane tube radius on permeate fraction and flow rate.
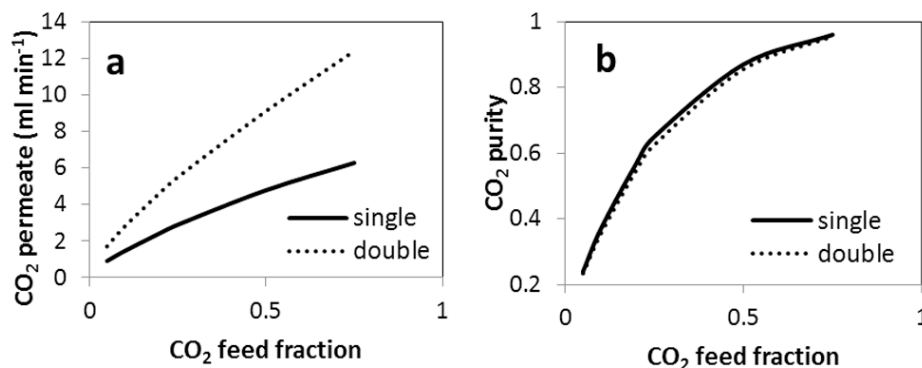

Figure 12: The effect of adding a new membrane in series.

shows CO_2 permeate flow rate in two different tube radiuses of 4.5 and 3 mm while molar flux of feeds remain constant in both cases, due to entrance tube radius is constant in both cases. As could be seen, CO_2 permeate flow rate decreases with decreasing the tube radius. The reason is decreasing the internal membrane area therefore less CO_2 can become in contact with membrane surface. In addition, Figure **11b** illustrates that permeate mole fraction remain constant with change in tube radius, because the driving forces for both gases remain constant.

Membranes in Series

To show the effect of adding a new membrane in series, some simulation with an additional membrane module were performed and results are shown in Figure **12**. It can be seen from Figure **12a** that due to connection of a new membrane and increase of membrane area more CO_2 permeate was resulted across the membrane, while according to Figure **12b** the purity of CO_2 was similar for double and single membranes. However, with permeation of more CO_2 from the membrane, driving force of CO_2 would be decreased, thus a slight decrease in CO_2 fraction for double membrane module could be seen.

CONCLUSIONS

In the present work, a CFD approach was used to simulate movement, diffusion and permeation of CO_2/CH_4 gaseous mixture through a tubular SAPO-34 membrane. Results showed good agreement with experimental outlet data for both components as a function of pressure drop along the membrane module. Concentration and velocity maps were obtained and concentration polarization effect was predicted in the feed side. The impact of operating conditions on separation were studied and showed that for enhancement of separation efficiency of CO_2 from CH_4, feed pressure, feed flow rate and tube radius and number of membrane modules in series should be increased, whereas flow configuration has less significant effect.

ACKNOWLEDGEMENTS

APPENDIX: NOMENCLATURE

A   Area (m^2)

b   parameter in Langmuir adsorption isotherm (pa^{-1})

D   Maxwell-Stefan diffusivity ($m^2 \ s^{-1}$)

D   Fick diffusivity ($m^2 \ s^{-1}$)

J   molar flux ($kmol \ m^{-2} \ s^{-1}$)

M   molecular weight ($kg \ kmol^{-1}$)

P   pressure (pa)

q   concentration of adsorbed gas ($kmol \ kg^{-1}$)

S   source/dink term ($kg \ m^{-3} \ s^{-1}$)

U   velocity vector ($m \ s^{-1}$)

V   volume (m^3)

Y   mass fraction (-)

Greek Symbols

δ   membrane thickness (m)

θ   coverage fraction (-)

ρ   density ($kg \ m^{-3}$)

τ   stress tensor (pa)

Subscripts

c   computational cell

feed   feed side

i   generic species

j   generic species

perm   permeation side

sat   saturation

z   zeolite film

REFERENCES

[1]   Baker RW. Future Directions of Membrane Gas Separation Technology. Ind Eng Chem Res 2002; 41(6): 1393-411. http://dx.doi.org/10.1021/ie0108088

[2]   Rufford TE, Smart S, Watson GCY, Graham BF, Boxall J, Diniz da Costa JC, *et al.* The removal of CO2 and N2 from natural gas: A review of conventional and emerging process technologies. J Pet Sci Eng 2012; 94-95: 123-54. http://dx.doi.org/10.1016/j.petrol.2012.06.016

[3]   Sridhar S, Smitha B, Aminabhavi TM. Separation of carbon dioxide from natural gas mixtures through polymeric membranes—A Review. Sep Purif Rev 2007; 36(2): 113-74. http://dx.doi.org/10.1080/15422110601165967

[4]   Hong M, Li S, Falconer JL, Noble RD. Hydrogen purification using a SAPO-34 membrane. J Memb Sci 2008; 307(2): 277-83. http://dx.doi.org/10.1016/j.memsci.2007.09.031

[5]   Krishna R, van Baten JM. Segregation effects in adsorption of CO2-containing mixtures and their consequences for separation selectivities in cage-type zeolites. Sep Purif Technol 2008; 61(3): 414-23. http://dx.doi.org/10.1016/j.seppur.2007.12.003

[6]   Ghidossi R, Veyret D, Moulin P. Computational fluid dynamics applied to membranes: State of the art and opportunities. Chem Eng Process 2006; 45(6): 437-54. http://dx.doi.org/10.1016/j.cep.2005.11.002

[7]   Fimbres-Weihs GA, Wiley DE. Review of 3D CFD modeling of flow and mass transfer in narrow spacer-filled channels in membrane modules. Chem Eng Process 2010; 49(7): 759-81. http://dx.doi.org/10.1016/j.cep.2010.01.007

[8]   Koukou MK, Papayannakos N, Markatos NC, Bracht M, Van Veen HM, Roskam A. Performance of ceramic membranes at elevated pressure and temperature: effect of non-ideal flow conditions in a pilot scale membrane separator. J Memb Sci. 1999; 155(2): 241-59. http://dx.doi.org/10.1016/S0376-7388(98)00315-9

[9]   Takaba H, Nakao Si. Computational fluid dynamics study on concentration polarization in H2/CO separation membranes. J Memb Sci 2005; 249(1-2): 83-8. http://dx.doi.org/10.1016/j.memsci.2004.09.038

[10]   Abdel-jawad MM, Gopalakrishnan S, Duke MC, Macrossan MN, Schneider PS, Diniz da Costa JC. Flowfields on feed and permeate sides of tubular molecular sieving silica (MSS) membranes. J Memb Sci 2007; 299(1-2): 229-35. http://dx.doi.org/10.1016/j.memsci.2007.04.046

[11]   Kawachale N, Kumar A, Kirpalani DM. Numerical Investigation of Hydrocarbon Enrichment of Process Gas Mixtures by Permeation through Polymeric Membranes. Chem Eng Technol 2008; 31(1): 58-65. http://dx.doi.org/10.1002/ceat.200700263

[12]   Coroneo M, Montante G, Catalano J, Paglianti A. Modelling the effect of operating conditions on hydrodynamics and mass transfer in a Pd-Ag membrane module for H2 purification. J Memb Sci 2009; 343(1-2): 34-41. http://dx.doi.org/10.1016/j.memsci.2009.07.008

[13]   Coroneo M, Montante G, Giacinti Baschetti M, Paglianti A. CFD modelling of inorganic membrane modules for gas mixture separation. Chem Eng Sci 2009; 64(5): 1085-94. http://dx.doi.org/10.1016/j.ces.2008.10.065

[14]   Ji G, Wang G, Hooman K, Bhatia S, Diniz da Costa JC. Simulation of binary gas separation through multi-tube molecular sieving membranes at high temperatures. Chem Eng J 2013; 218: 394-404. http://dx.doi.org/10.1016/j.cej.2012.12.063

[15]   Ji G, Wang G, Hooman K, Bhatia S, Diniz da Costa JC. The fluid dynamic effect on the driving force for a cobalt oxide silica membrane module at high temperatures. Chem Eng Sci 2014; 111: 142-52. http://dx.doi.org/10.1016/j.ces.2014.02.006

[16]   Li H, Schygulla U, Hoffmann J, Niehoff P, Haas-Santo K, Dittmeyer R. Experimental and modeling study of gas

transport through composite ceramic membranes. Chem Eng Sci 2014; 108: 94-102.
http://dx.doi.org/10.1016/j.ces.2013.12.030

[17]   Jabbari Z, Fatemi S, Davoodpour M. Improvement of SAPO-34 fine layer formation on ceramic and steel supports by applying uniform-size synthesized seed particles. Asia-Pac J Chem Eng 2013; 8(2): 301-10.
http://dx.doi.org/10.1002/apj.1682

[18]   Jareman F, Hedlund J, Creaser D, Sterte J. Modelling of single gas permeation in real MFI membranes. J Memb Sci 2004; 236(1-2): 81-9.
http://dx.doi.org/10.1016/j.memsci.2004.01.028

[19]   Nagy E. Basic Equations of the Mass Transport through a Membrane Layer. First ed. Oxford: Elsevier; 2012. 330 p.

[20]   Wirawan SK, Creaser D, Lindmark J, Hedlund J, Bendiyasa IM, Sediawan WB. H2/CO2 permeation through a silicalite-1 composite membrane. J Memb Sci 2011; 375(1-2): 313-22.
http://dx.doi.org/10.1016/j.memsci.2011.03.061

[21]   Martinek JG, Gardner TQ, Noble RD, Falconer JL. Modeling Transient Permeation of Binary Mixtures through Zeolite Membranes. Ind Eng Chem Res 2006; 45(17): 6032-43.
http://dx.doi.org/10.1021/ie060166u

[22]   Ansys Fluent User's Guide, Release 13.0: Ansys Inc.; 2010.

[23]   Li S, Falconer JL, Noble RD, Krishna R. Modeling Permeation of CO2/CH4, CO2/N2, and N2/CH4 Mixtures Across SAPO-34 Membrane with the Maxwell−Stefan Equations. Ind Eng Chem Res 2007; 46(12): 3904-11.
http://dx.doi.org/10.1021/ie0610703